Guidance, Navigation, and Control and Co-located Conferences
August 19-22, 2013, Boston, MA
AIAA Guidance, Navigation, and Control (GNC) Conference

Observed Time Difference of Arrival/GPS Fusion for Urban UAS Navigation using Particle Filtering Techniques

Justin R. Rufa*and Ella M. Atkins†
University of Michigan, Ann Arbor, MI, USA

As Unmanned Aircraft Systems (UAS) become more accepted into our society, law enforcement, emergency services, and commercial entities will begin taking advantage of this technology in high-population urban settings. Since these aircraft will be operating between and above the high-rise buildings that define most urban cores, increased position estimation accuracy will become paramount to ensure safe and reliable operations. Fighting against this need for better accuracy is the degradation of Global Positioning System (GPS) accuracy in urban canyons due to signal reflection and refraction caused by buildings and other tall objects. UAS cannot rely solely on GPS position measurements for guidance and navigation to effectively conduct urban missions. A potential solution to achieve the necessary positioning accuracy is through the fusion of the GPS data with cellular Observed Time Difference of Arrival (OTDOA) position measurements. In areas with even modest GPS coverage, today's smart phones are already equipped to provide both measurements thus could plug into a UAS to serve as the low-cost urban autopilot of the future. Because OTDOA data is noisy, data filtering and fusion is essential. This paper proposes a sampling importance resampling particle filter to estimate UAS position from GPS and OTDOA data. Expected data error statistics are summarized from the literature and used in simulation to evaluate positioning accuracies using GPS alone, OTDOA alone, and a fusion of both data sources. Results show the GPS augmented by OTDOA provides a more accurate estimate of UAS position than either alone. However, OTDOA measurements from cellular networks of today are not as accurate as GPS measurements, thus are not yet a good sole source of aircraft position measurements, suggesting augmentation by another secondary sensing source distinct from GPS in GPS-denied areas in future work.

Nomenclature

$\hat{x}$ particle mean
μ_z sensor mean error
σ_j particle roughening standard deviation
σ_z sensor error standard deviation
c speed of light
d_i distance from base station to cellular device
E distance betwen min and max particles
H measurement availability value
h constant difference hyperbola
J jitter covariance matrix
j particle roughening
K constant tuning parameter
N number of particles
n number of hearable base stations

*PhD Student, Aerospace Engineering, AIAA Student Member
†Associate Professor, Aerospace Engineering Dept., AIAA Associate Fellow

P particle covariance matrix
Q number of sensors
r state space dimension
s distance from particle to measurement
u control input
v measurement noise
w particle weight
X particle set
x particle
z measurement
$\tilde{x}$ true aircraft state
ξ process noise

I. Introduction

As Unmanned Aircraft Systems (UAS) technology continues to mature, Federal Aviation Administration (FAA) rules will be crafted to enable UAS integration in the National Airspace System (NAS). As the price to fly small UAS decreases, civilian government, law enforcement, and other non-military entities will have the capabilities to conduct urban small UAS missions in urban areas. Potential missions include urban law enforcement, anti-terrorism, riot control, traffic surveillance, natural disaster monitoring, emergency medical/flood delivery, and communications relay.[1] In fact, law enforcement in the United States, Canada, and Europe have already begun to determine how UAS can fit into their missions.

As early as 2007, the United Kingdom was investigating requirements necessary for UAS to augment manned aircraft conducting urban law enforcement missions. One of the challenges specifically cited was sensor obscuration, which further shows the need for navigation and control systems independent of any one data source.[2] In Canada, the Ontario Provincial Police have already taken advantage of a Special Flight Operations Certificate to operate UAS in a law enforcement role across the province, including urban areas.[3] The Seattle, Washington Police Department have also received FAA permission to operate a drone that will be used primarily for traffic accident surveillance and possible hostage situations in and around buildings before the drone program was abruptly canceled over privacy concerns.[4]

The importance of these types of missions, especially in time-sensitive law enforcement and emergency situations, require navigation and guidance systems be sufficiently robust to handle sensor anomalies common in urban canyons, including degradation/loss of GPS (Global Positioning System) position/altitude/velocity data. Robust navigation will be necessary to ensure both the safety of people on the ground (pedestrians and vehicle traffic), and to avoid damage to both public infrastructure and private property.

Completing these urban missions depends on having a reliable navigation system, including a reliable GPS signal, if it is to be used as the primary geolocation source. Even though this technology is sometimes taken for granted, GPS may be severely degraded or unavailable due to phenomena such as free space loss, refraction/absorption in the atmosphere, and both reflection and masking from urban structures, foliage, and other environmental factors.[5] In urban areas where the GPS signal is available, multipath and masking contribute to an increased geometric dilution of precision of the measurements.[6] A GPS accuracy experiment on Hong Kong in 2007 demonstrated how the signal is degraded within an urban canyon. In the experiment, only 50% of the area studied had adequate GPS reception to produce a measurement. Of that area, 40% of the test points showed errors greater than 20 meters and 9% showed errors in excess of 100 meters.[7] This level of availability and accuracy is not sufficient for a GPS receiver to be the primary navigation sensor in an urban canyon.

In 2007, the Defense Advanced Research Projects Agency, concerned by the possibility of losing GPS navigation capabilities, funded a Robust Surface Navigation program that studied how navigation could continue without using GPS signals. It examined "signals of opportunity," including cell phone towers, television and even other satellites, to determine if they would be viable for navigation purposes.[8] Rockwell Collins also investigated ways to conduct UAS missions in GPS-denied urban canyons, reaching the conclusion that only a multi-sensor solution would give the accuracy needed.[9]

In mid 2012, BAE Systems announced that it has been developing a technology called Navigation via Signals of Opportunity (NAVSOP) to allow for navigation using various electromagnetic signals already existing in the environment. These emanate from GPS satellites, GPS jamming devices, air traffic control

communications, as well as television, cell phone, and radio communication towers. A key advantage of the system is that it can provide navigation capabilities where GPS is either degraded or unavailable, including urban canyons.[10] Many signals are already available for navigation, but the challenge currently lies in the development of the hardware to exploit these signals.

The goal of this paper is to develop a small UAS navigation scheme that can estimate 2-D lateral ($\tilde{x}_{North}$, $\tilde{x}_{East}$) trajectory through an urban canyon, initialized from a location within a 30m x 30m grid, using particle filtering techniques to fuse measurements from multiple sensors. The main contribution of this paper is the characterization of this 2-D position error over time using GPS and Observed Time Difference of Arrival (OTDOA) measurements. It will be assumed that the altitude/height of the UAS can be measured independently using pressure sensing for Mean Sea Level measurements or height sensing for Above Ground Level measurements.

The rest of the paper is as follows. Section II discusses several standardized cellular network mobile device geolocation techniques, focusing on OTDOA, introduces the UAS dynamics model, and then gives an overview on the fundamentals of particle filtering. It concludes with a flow diagram of the 2-D position estimation algorithm. Section III gives the simulation parameters, GPS and OTDOA accuracy characteristics, and discusses aircraft position estimation in terms of particle prediction and update. Section IV gives the results of the simulation, in terms of 2-D error, using the sensors individually and then combining the GPS and OTDOA measurements for fused results. It also analyzes the trends in the results to determine which factors have the biggest impact on the accuracy. Section V concludes the paper.

II. Background

A. Cellular Network Mobile Device Geolocation Techniques

There are several different types of geolocation techniques currently available to pinpoint the location of a mobile device. Many of these techniques are shown in Figure 1 as a function of their response time and position accuracy. The arrow represents the tradeoff between accuracy, typically in meters, and response time, typically in seconds, of the various techniques. The techniques fall into four broad categories. The first category is Enhanced Cell ID (E-CID). The main characteristic of E-CID is the use of the current base station location as an estimate of the location of the device. The second is Time Difference of Arrival (TDOA). TDOA techniques use the time difference between reference signals sent from multiple base stations to the mobile device (OTDOA) or signals sent from the mobile device to multiple base stations to determine its location (Uplink-TDOA). The third is Assisted-Global Navigation Satellite Systems (A-GNSS). A-GNSS uses satellite signals (normally GPS) to determine the device's location, but A-GNSS is hampered by longer time to first fix (TTFF) and shorter battery life for the device as compared to the other techniques.[11] Radio Frequency (RF) fingerprinting, also known as the Database Correlation Method or Adaptive Enhanced Cell ID (AECID), uses cellular network signal strength information for various cellular towers as a way of geolocating the device. It relies on the fact that signal strengths from different towers are generally consistent from day to day in the same location. The AECID version of this technique also uses Cell IDs, timing advances, angle of arrival, and reference signal time difference in addition to the signal strengths.[12]

Each of the cellular geolocation techniques are optimized for different environments and applications. In the case of providing a measurement estimation for a UAS in an urban canyon, accuracy is the most important characteristic of the estimation. This leads to A-GNSS, OTDOA, or Uplink-TDOA as the best candidates. The accuracy advantage of A-GNSS is negated in urban environments when the position data is either highly inaccurate or not available at all. Another consideration is that not all current mobile devices are built with an installed GPS receiver. This leaves Uplink-TDOA and OTDOA remaining. Uplink-TDOA, set to be defined in Release 11 as an additional 3GPP LPP technique, is the fully network-based version of OTDOA. The benefit of this technique is that it requires no modifications to user equipment, making implementation seamless to mobile device users. However, it requires location measurement units (LMUs) on each base station and is mostly proprietary so accuracy data for Uplink-TDOA is not available to the public[12,13]. This leaves OTDOA as the most accurate technique universal to all mobile devices. This method is becoming more popular with cellular network carriers because the network-based version requires no modifications to LTE (Long Term Evolution)-capable mobile devices.[14] Accuracy of this technique also increases as a function of hearable towers, which is generally maximized in urban areas.

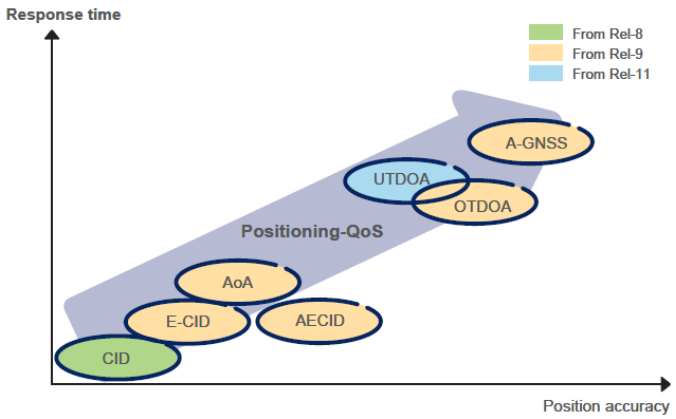

Figure 1. Cellular Geolocation Techniques from Ericsson[12]

Observed Time Difference of Arrival

The OTDOA geolocation technique, shown in Figure 2, was first officially defined in the 3GPP TS 36.355 Release 9 as one of the three LTE Positioning Protocol (LPP) techniques.[15] It uses multilateration (hyperbolic lateration) to find a mobile device with either the mobile device completing the calculations or the network completing the calculations. In order for the mobile device calculation mode to be accurate, the following conditions must be met. First, the mobile device must have a priori knowledge of the 2-D coordinates of all base stations in its operating area. Second, all base stations in the operating area must be synchronized with each other, but do not need to be synchronized with mobile device.

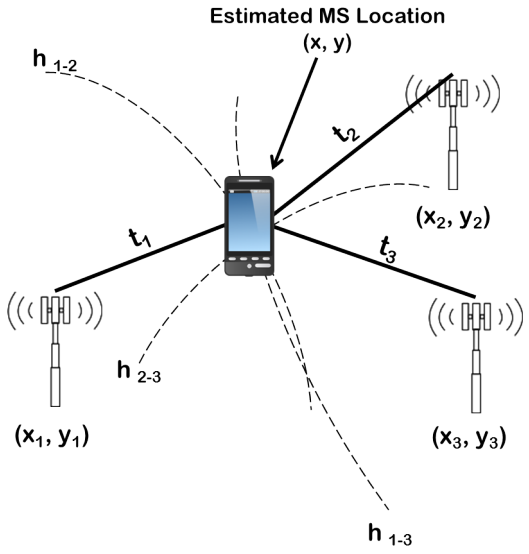

Figure 2. OTDOA Geolocation Technique

The OTDOA process starts when a position reference signal (PRS) is sent from n base stations to the mobile device, where $n > 3$. Once the device timestamps the arrival times of the n signals, these measurements are sent to a location server on the network where the difference between each pair of arrival times $(t_2 - t_1)$ is calculated. These time differences are converted to distance differences by multiplying the time differences by c, the speed of light, as shown in (1).

$$d_{i+1} - d_i = c * (t_{i+1} - t_i) \tag{1}$$

Each constant distance difference forms a hyperbola (h_{1-2}) between the two base stations that contains the estimated position of the device. To narrow its location to a maximum of two points along h_{1-2}, a second hyperbola is drawn (h_{1-3}).[16] If the two hyperbolas only intersect in one location, then the estimated device location is that point of intersection. However, as Figure 2 shows, sometimes h_{1-2} and h_{1-3}intersect at two points, making a third hyperbola necessary. The intersection of this third hyperbola (h_{2-3}), along with the first two hyperbolas, completely defines the estimated location of the device.[17] The estimated location can then be determined by solving a system of three non-linear equations simultaneously.

Solving three non-linear equations simultaneously requires the use of numerical methods. When $n = 3$ (i.e., three base stations hearable to the device), then this is the only option for calculating the device's position. However, when $n \geq 4$, the system of equations can be linearized and solved using matrix operations for most base station layouts.

The non-linear method requires solving the system of three non-linear equations, shown in (2), simultaneously for x and y, using a numerical solver.

$$\begin{aligned} d_2 - d_1 &= \sqrt{(x_2 - x)^2 + (y_2 - y)^2} - \sqrt{(x_1 - x)^2 + (y_1 - y)^2} \\ d_3 - d_1 &= \sqrt{(x_3 - x)^2 + (y_3 - y)^2} - \sqrt{(x_1 - x)^2 + (y_1 - y)^2} \\ d_3 - d_2 &= \sqrt{(x_3 - x)^2 + (y_3 - y)^2} - \sqrt{(x_2 - x)^2 + (y_2 - y)^2} \end{aligned} \tag{2}$$

There are several iterative algorithms that can solve this system of non-linear equations, including the Levenberg-Marquardt, Gauss-Newton, and Steepest Descent algorithms, discussed in Mensing and Plass.[18] Another iterative algorithm that addresses a moving source is the Constrained Weighted Least Squares algorithm.[19] While this method is able to accurately geolocate a UAS using only three towers, as a numerical solver, it may not be able to reach a solution as quickly as other methods. While three towers are theoretically sufficient, results may also be inaccurate due lack of precision in the data. Use of additional towers when available can therefore offer substantial improvement in position estimates.

The linear technique can be used if the device is able to hear four or more base stations. The 2-D linear geolocation equations for n towers are shown in (3) - (7). Note that $m = \{3, 4, ..., n\}$. The complete three dimensional derivation is available in Bucher and Misra.[20]

$$A_m x + B_m y + D_m = 0 \tag{3}$$

$$A_m = \frac{2x_m}{d_m - d_1} - \frac{2x_2}{d_2 - d_1} \tag{4}$$

$$B_m = \frac{2y_m}{d_m - d_1} - \frac{2y_2}{d_2 - d_1} \tag{5}$$

$$D_m = d_m - d_1 - (d_2 - d_1) - \frac{x_m^2 + y_m^2}{d_m - d_1} - \frac{x_2^2 + y_2^2}{d_2 - d_1} \tag{6}$$

$$\begin{bmatrix} x \\ y \end{bmatrix} = - \begin{bmatrix} A_3 & B_3 \\ \vdots & \vdots \\ A_n & B_n \end{bmatrix}^{\dagger} \begin{bmatrix} D_3 \\ \vdots \\ D_n \end{bmatrix} \tag{7}$$

The estimated device location is found by solving (7) using matrix operations. Multiple works verify that in situations where $n > 4$, the accuracy of the TDOA method increases as the number of towers (and therefore number of equations) increases.[13,21]

B. Aircraft Model

The UAS equations of motions, shown in (8), were developed for a 28 kg fixed wing aircraft in Moeckli.[22] The model was developed using the North-East-Down navigation frame for aircraft position, the aircraft body frame and aircraft wind frame for airspeed, and both Euler angles (shown here) and quaternions for aircraft attitude. The quaternions eliminate Euler angle singularity issues when the aircraft's pitch approaches 90 degrees.

$$\begin{aligned}
\begin{bmatrix} \dot{x}_N \\ \dot{x}_E \\ \dot{x}_D \end{bmatrix} &= C_b^n \begin{bmatrix} u \\ v \\ w \end{bmatrix} \\
\begin{bmatrix} \dot{u} \\ \dot{v} \\ \dot{w} \end{bmatrix} &= \tfrac{1}{m} \left(C_w^b \begin{bmatrix} X^w \\ Y^w \\ Z^w \end{bmatrix} + \begin{bmatrix} F_T \\ 0 \\ 0 \end{bmatrix} \right) + C_n^b \begin{bmatrix} 0 \\ 0 \\ g \end{bmatrix} + \begin{bmatrix} u \\ v \\ w \end{bmatrix} \times \begin{bmatrix} p \\ q \\ r \end{bmatrix} \\
\begin{bmatrix} \dot{\phi} \\ \dot{\theta} \\ \psi \end{bmatrix} &= \begin{bmatrix} 1 & tan\,\theta sin\,\phi & tan\,\theta cos\,\phi \\ 0 & cos\,\phi & -sin\,\phi \\ 0 & sin\,\phi/cos\,\theta & cos\,\phi/cos\,\theta \end{bmatrix} \begin{bmatrix} p \\ q \\ r \end{bmatrix} \\
\begin{bmatrix} \dot{p} \\ \dot{q} \\ \dot{r} \end{bmatrix} &= I^{b^{-1}} \left(\begin{bmatrix} L^b \\ M^b \\ N^b \end{bmatrix} - \begin{bmatrix} p \\ q \\ r \end{bmatrix} \times I^b \begin{bmatrix} p \\ q \\ r \end{bmatrix} \right)
\end{aligned} \tag{8}$$

The full derivation of the model can be found also be found in Moeckli.[22] It includes the aircraft's physical parameters as well as the derivatives needed to calculate forces and moments. This model is assumed to be valid only in prestall conditions since lift is modeled as a linear function of angle of attack.

C. Sampling Importance Resampling Particle Filter

This research will focus on using a Sampling Importance Resampling (SIR) particle filter and particle roughening (also known as jitter), both introduced in Gordon et al[23] to estimate the UAS 2-D position. The basic idea of the SIR is to sample N particles from the posterior density distribution shown in (9) at each time step as a discrete approximation. Thrun et al[24] describes each of the particles, $\mathbf{x}_k^i$, as a hypothesis or concrete instantiation of the state at time k, given measurements, $\mathbf{z}_{1:k}$, and control inputs, $\mathbf{u}_{1:k}$. With enough samples, the particle set, $\mathbf{X}_k = \{x_k^1, x_k^2, x_k^3, ..., x_k^N\}$, will accurately approximate the posterior density.

$$\mathbf{x}_k^i \sim p(\mathbf{x}_k | \mathbf{z}_{1:k}, \mathbf{u}_{1:k}) \tag{9}$$

Similar to other Bayesian filters, the SIR particle filter uses a prediction step and an update step, with the addition of a resampling step. The importance density, $q(\mathbf{x}_k | \mathbf{x}_{k-1}^i, \mathbf{z}_{1:k})$, is chosen to be the prior density, $p(\mathbf{x}_k | \mathbf{x}_{k-1}^i)$, which affects both the prediction and update steps.

1. *Prediction*

As the system's state evolves over time, the particle filter samples from the importance density, which is chosen as the prior density in the SIR. Samples are drawn from the prior by propagating each particle forward using the noisy dynamics of the system, shown in (10), with process noise indicated as ξ_{k-1}^i.

$$\mathbf{x}_k^i = f_k(\mathbf{x}_{k-1}^i, \mathbf{u}_{k-1}, \xi_{k-1}^i) \tag{10}$$

2. *Update*

Once the particles have been propagated to the current time step for each state, they must be assessed to determine their accuracy given the current measurements. Each of sensor measurement, $\mathbf{z}_k$, is generated according to (11) where $\tilde{\mathbf{x}}_k$ is the true state of the system at time-step k and $\mathbf{v}_k$ is Gaussian noise drawn from $\mathcal{N}(\mu_Z, \sigma_z^2)$.

$$\mathbf{z}_k = \tilde{\mathbf{x}}_k + \mathbf{v}_k \tag{11}$$

Weights are assigned to each particle using (12), with the derivation, including the effect of the importance density choice and resampling step, found in Arulampalam et al.[25]

$$w_k^i = p(\mathbf{z}_k|\mathbf{x}_k^i) \tag{12}$$

After the weights of the particles are normalized, the SIR particle filter resamples the particles to avoid degeneracy. Degeneracy occurs when most of the particles have very small weights and only a few particles have large enough weights to influence the estimate. By continuing to carry the lower weighted particles, the algorithm runs less efficiently since computational resources being spent on these lower weighted particles. Techniques such as resampling help alleviate this problem.[26] According to Ristic et al,[27] the weighted particle mean and covariance should be calculated immediately after normalizing the particle weights if they are to be used to characterize the estimate of (9). This is due to an increase in the variance of the posterior distribution during the resampling stage, as explained in Carpenter et al.[28]

3. Resampling

Resampling is the process by which lower weighted particles are replaced by copies of the higher weighted particles to create an independent and identically distributed representation of the posterior density. The resampling algorithm in Arulampalam et al[25] starts by calculating a cumulative distribution function (CDF) for $i = 2 : N$, using (13),where $\overline{c}_1 = 0$.

$$\overline{c}_i = \overline{c}_{i-1} + w_k^i \tag{13}$$

After i is reinitialized to 1,a starting point is selected from (14).

$$\overline{u}_1 \sim U(0, N^{-1}) \tag{14}$$

This starting point, $\overline{u}_1$, is compared to increasing values of $\overline{c}_i$ by continually moving up the CDF. Once $\overline{c}_i$ becomes greater than or equal to $\overline{u}_1$, the first particle is set equal to $x^i$and its weight is set to N^{-1}. The next starting point, $\overline{u}_2$,is calculated using (15), and the process repeats until all particles have been assigned resampled values

$$\overline{u}_j = \overline{u}_1 + N * (j-1) \tag{15}$$

One of the issues with resampling is that the same particle may be selected several times, leaving the distribution represented by only a few distinct particles. This is known as sample impoverishment. Sample impoverishment tends to become more of a problem in dynamic systems with small process noise.

4. Particle Roughening

Particle roughening (also known as jittering) is a technique that gives a more diverse particle distribution after resampling.[23] It can be used as the last step in a SIR particle filter when the system has small process noise and suffering from sample impoverishment. Roughening moves each particle slightly, giving N unique particles to represent the posterior. The amount each particle is moved, j_k^i, is drawn from $\mathcal{N}(0, J)$, where J is the diagonal roughening covariance matrix. The standard deviations are calculated using (16) where K is a user-selected constant tuning parameter, E is the distance between the minimum and maximum values of the state, and r is the dimension of the state space.

$$\sigma_j = KEN^{-1/r} \tag{16}$$

D. Fusing Sensor Data in Particle Filter

If Q sensors are available to collect mutually-independent measurements, each measurement must be appropriately weighted when used in the particle filter. Khan et al[29] suggests the weight of a likelihood function for the q^{th} sensor as:

$$w_k^{i,q} \propto p(\mathbf{z}_k^q|\mathbf{x}_k^i) \tag{17}$$

Since each of the sensors are independent, the joint likelihood of the multiple measurements given a particle is simply the product of the individual likelihoods as shown in (18).

$$p(\mathbf{z}_k|\mathbf{x}_k^i) = p(\mathbf{z}_k^1|\mathbf{x}_k^i), p(\mathbf{z}_k^2|\mathbf{x}_k^i), ..., p(\mathbf{z}_k^q|\mathbf{x}_k^i) \tag{18}$$

Equating (12) and (18) gives the pre-normalized weight of each particle as the product of the individual weights for each particle, shown in (19).[30]

$$w_k^i \propto \prod_{q=1}^{Q} p(\mathbf{z}_k^q|\mathbf{x}_k^i) \tag{19}$$

Figure 3 summarizes the particle filtering process flow in terms of prediction, update, resample, and roughening of the particles and how the particle weights change at different steps of the process. The solid line indicates the flow for a time-step with at least one available measurement. When a measurement is not available, the update and resample steps are omitted as indicated by the dashed lines.

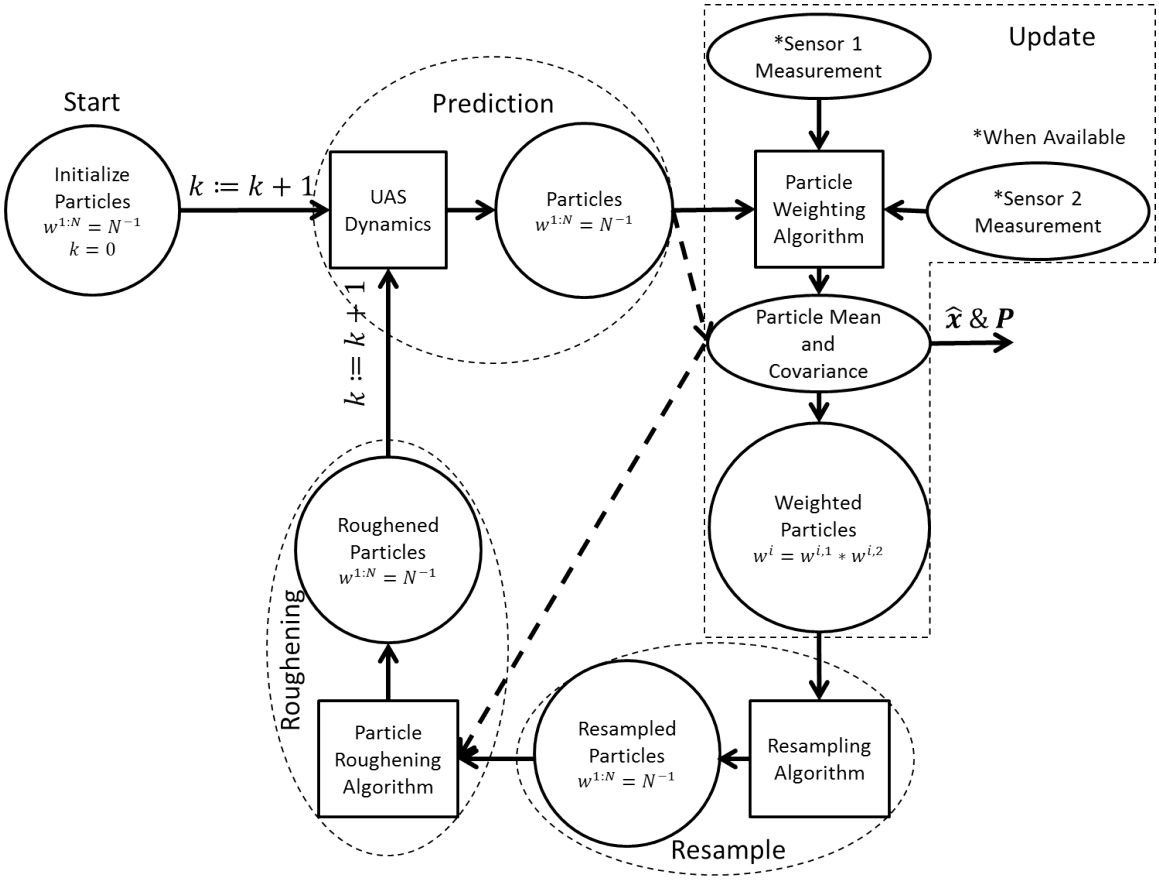

Figure 3. SIR Particle Filter Flow Diagram

III. Simulation

A 2-D lateral trajectory estimation simulation was developed in MATLAB using the UAS dynamics and a SIR particle filter with roughening. The constants for the simulation are shown in Table (1). By running the simulation 100 times at each test point, each of the distributions should have been sufficiently sampled to attain consistent state estimates and error estimates.

Constant Tuning Parameter,[23] K	0.2
Number of Monte Carlo Runs	100
Number of Particles, N	100
Simulation Length	$20s$
Time-Step, dt	$0.1s$

Table 1. Simulation Parameters

A. Sensor Measurement Availability

GPS measurements were sampled at 5Hz[31]and OTDOA measurements were sampled at 5Hz, 2.5 HZ, and 1Hz. The 5Hz OTDOA update rate was selected to show the potential geolocation accuracy should this technology achieve rates comparable to fast GPS refresh rates. The 2.5 Hz update rate was a tradeoff between 5Hz and 1Hz GPS receivers. Since Polaris Wireless is currently working on a 1Hz geolocation solution, it was selected to show the results of current OTDOA accuracies combined with this sampling rate.[32] Sensor latency was assumed to be zero, but effective sampling rate was varied as described below.

To best replicate real-world conditions and performance of the sensors, both the GPS and OTDOA sensors measurements were not sampled at the exact rate, but varied during each run. For each time step, the sensor was assigned an availability value from the distribution in (20).

$$H \sim \mathcal{U}(0,1) \tag{20}$$

This value was compared to the product of the sensor sampling rate, in Hz, multiplied by the time-step length, as shown in (21).

$$H \leq sample\,rate * dt \tag{21}$$

For time-steps when (21) was satisfied, the measurement was reported. Conversely, when it was not satisfied, the measurement was not reported.

B. Sensor Measurement Error Characteristics

1. *Urban GPS*

The urban GPS error data used for this research was taken from McGougan et al during a driving experiment in downtown Vancouver on October 13-14, 2001.[33] Vancouver was selected as one of the cities for their experiment due to its dense core of high rise buildings. As shown in Table 2, the experiment showed the difficulty in accurate geolocation in these environments with the worse receiver having a 3σ error of roughly 70.7 meters. Even the best performing GPS receiver in this experiment had a 3σ error of 30.3 meters.

Table 2. Urban GPS 2-D Measurement Error Statistics

Sensor	GPS, HS SiRF14	GPS, HS SiRF66	GPS, ST SiRF30
Mean, μ (meters)	12.5	11.9	7.8
Standard Deviation, σ (meters)	19.4	17.9	7.5

2. *OTDOA*

OTDOA accuracy data can be difficult to collect experimentally because it requires specialized communications with the network as well as access to a network's location server when using the mobile device-assisted mode. Because of this, the available data is typically simulation-based. Ahonen et al's accuracy data was characterized as a cumulative density function curve as shown in Figure 4.[34]

Neuland et al[35] and Tao[36] characterized their accuracy data as a Gaussian distribution. Accuracy characteristics for each source are summarized in Table 3.

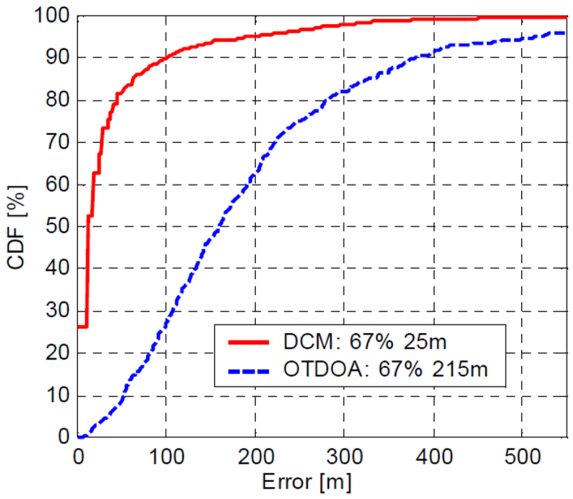

Figure 4. OTDOA CDF Curve from Ahonen[34]

Table 3. OTDOA 2-D Measurement Error Statistics

Sensor	Ahonen et al	Neuland et al	Tao
Mean, μ (meters)	215 (67%)	16.3	45.54
Standard Deviation, σ (meters)	N/A	31.4	2.65

The curve fit approximation for Ahonen is $F(x) = -1.96*10^{-13}x^5+3.12*10^{-10}x^4-1.78*10^{-7}x^3+3.84*10^{-5}x^2+0.00044x-0.003438$, and was used to generate the distribution in Figure 5a. Figures 5a-5c show 100 measurements taken from each of the three distributions. Figure 5a shows large variation in measurement errors that range from 0 to 500 meters in either direction, while Figure 5b shows variations only up to 80 meters in either direction. Figure 5c measurements are always offset from the true location by roughly the mean value across all angles suggesting that the simulation had a bias but produced precise measurements.

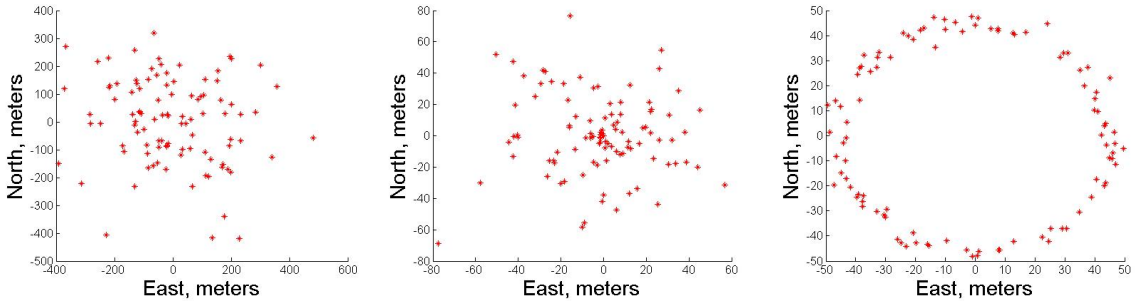

a) Ahonen: CDF **b) Neuland et al:** $\mu = 16.3m$; $\sigma = 31.4m$ **c) Sensor 3:** $\mu = 45.54m$; $\sigma = 2.65m$

Figure 5. OTDOA Measurement Distributions from Literature

The SiRF30 GPS receiver (from Table 2) was used for the simulation, due to its accuracy, along with the Neuland et al (OTDOA 1) and Tao (OTDOA 2) accuracy characterizations (from Table 3). Since the errors are reported as a lateral range, rather than in the x_N and x_E directions, further analysis was completed to calculate the mean and standard deviation for each components. This allowed for independent measurements in each direction. The first and second calculated moments are shown in Table 4.

Table 4. GPS and OTDOA Lateral Component Measurement Error Characterization

	GPS		OTDOA 1		OTDOA 2	
	$\tilde{x}_N$	$\tilde{x}_E$	$\tilde{x}_N$	$\tilde{x}_E$	$\tilde{x}_N$	$\tilde{x}_E$
$\mu_z(m)$	0.0065 m	-0.0044 m	0.0271 m	-0.0112 m	-0.0847 m	0.0063 m
$\sigma_z(m)$	7.6572 m	7.6546 m	25.0061 m	25.0420 m	32.261 m	32.2511 m

C. UAS Position Estimation using a Sampling Importance Resampling Particle Filter

1. *Prediction*

This work assumed that the aircraft non-linear dynamics are noise-free and that the UAS states propagated exactly according to (8) for each particle. This noise-free propagation gives a starting point for analysis, with process noise tuning as a topic for future work. The UAS state was initialized[a] to:

$$\tilde{x}_0 = [-15\ -15\ -50\,29.42750\,2.79\,0\,0\,0\,0\,0\,0\,60]^T$$

The initial particles for the 2-D position estimate, $\{x_N x_E\}$, were drawn from a uniform distribution within a 30 meter by 30 meter 2-D box centered at the origin to represent the size of a large city intersection. Once the initial particles were generated, the system dynamics were propagated forward using a Runge-Kutta fourth order technique from Matthews.[37]

2. *Update*

When measurements were available, the likelihoods, which were used as the particles weights, were calculated using the normal distribution probability distribution function, shown in (22), where s^i was the measured distance between the current measurement and each particle.

$$p(\mathbf{z}_k^q|\mathbf{x}_k^i) = \frac{1}{\sigma_z^q\sqrt{2\pi}} exp\{\frac{-(s^i-\mu_z^q)^2}{2(\sigma_z^q)^2}\} \tag{22}$$

When multiple sensors produced a measurement at a given time-step, the two sets of likelihoods were fused together using (19) to produce a single weight for each particle. After the particles weights were normalized, the particle mean, $\hat{x}$, and covariance matrix,P, were calculated.

Resampling and roughening followed, ensuring that the filter would propagate 100 unique particles, representing the posterior, at each time step. When no measurements were available at a time-step, the particle mean and covariance was calculated immediately after the prediction step, the update and resampling step were omitted, and the particles were roughened.

IV. Results and Analysis

Results are shown for both single sensor cases and sensor fusion cases. All trajectories are shown with the true state in blue, the state estimate in green, the lower 3σ uncertainty bound in red, and the upper 3σ uncertainty bound in cyan. The first plot in each grouping contains a legend for ease of reading. Time history root mean square error plots are shown for all single sensor cases except 1Hz, but not for the sensor fusion cases, since all are similar to the GPS-5Hz case. Table data includes root mean square error for each case as well as the effective sampling rate for each sensor in each case. Since plots for $\tilde{x}_E$ show similar trajectory and RMS error trends as for $\tilde{x}_N$, they are not displayed.

A. Single Sensor - GPS or OTDOA

Figure 6 shows the $\tilde{x}_N$ state estimate using GPS at 5Hz and Figure 7 shows the $\tilde{x}_N$ state estimate using OTDOA 1 at 5 Hz (Figure 7a) and 2.5Hz (Figure 7b). Figure 8 shows the $\tilde{x}_N$ state estimate using OTDOA 2 at 5 Hz (Figure 8a) and 2.5Hz (Figure 8b). The state estimate mean value stays very close to the true value in all cases, with each of the 5Hz figures showing fairly stable uncertainty bounds with only one large

[a]Velocity components and engine RPM were provided in an e-mail from Dr. Guillaume Ducard dated 10/19/2012.

spike in the OTDOA 1 case. For the 2.5 Hz sampling rate, the uncertainty bounds have large spikes along the full length of the simulation for both OTDOA cases. These spikes indicate rapidly widening particle distributions, which occur due to the lack of measurements and are corrected once a measurement is received. Overall, when only one sensor is used, the uncertainty bounds do not converge towards the state estimate, meaning that the particle distribution is not able to tighten around the true state and provide increasing confidence in the estimate.

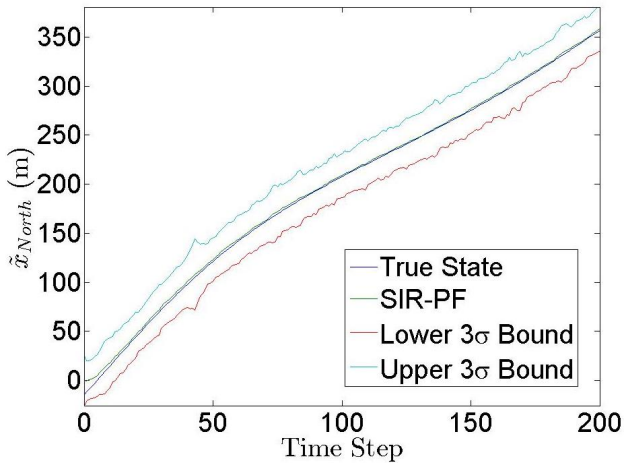

Figure 6. GPS $\tilde{x}_N$ Estimate - 5Hz

The single sensor RMS error means are summarized in Table 5 to allow for quantitative comparisons between different sensors and filters. These values are related to both the measurement sampling rate and the standard deviation of the measurement error. GPS gives the most accurate results at 5Hz with slightly greater than five meter error. OTDOA 1 gives three times more error at 5Hz and six to eight times more error at 2.5Hz. OTDOA 2 gives four times more error at 5Hz and six times more error at 2.5Hz.

In the 1Hz case, neither OTDOA 1 nor OTDOA 2 are able to estimate the state of the UAS using the SIR particle filter based on their RMS error values. The main reason for this divergent behavior is lack of measurements. In the 1Hz case, the particle filter only has one measurement every ten seconds that is used to correct the estimate. As the state propagates without a measurement, the particle distribution moves away from the true state. When the measurement is finally received, it cannot correct the particle trajectories if they are all arbitrarily far from the true value since they are all weighted equally and all are resampled as a result. This behavior causes the distribution to move away from the true state without bound until the errors grow to be large values approximating infinity.

The $\tilde{x}_N$ RMS error is larger than the $\tilde{x}_E$ in all but the OTDOA 2 2.5 Hz case. This difference is expected due to the slightly smaller measurement error means in the $\tilde{x}_E$ direction for all sensors.

Table 5. RMS Error Mean for Standalone GPS and OTDOA Sensors

	GPS		OTDOA 1		OTDOA 2	
	$\tilde{x}_N$	$\tilde{x}_E$	$\tilde{x}_N$	$\tilde{x}_E$	$\tilde{x}_N$	$\tilde{x}_E$
5Hz	5.3853 m	5.0529 m	15.8836 m	15.2966 m	20.1001 m	19.8139 m
2.5Hz	N/A	N/A	39.7450 m	29.8456 m	31.4472 m	31.6479 m
1Hz	N/A	N/A	396.07K m	240.89K m	1,618.4K m	1,371K m

Figure 9 shows the RMS error values for OTDOA 1 compared to GPS and Figure 10 shows the RMS error values for OTDOA 2 compared to GPS. Both show relatively steady values for GPS and OTDOA when measurements are sampled at 5Hz. However, the 2.5Hz OTDOA cases show spikes with an increasing stead-state values. These spikes occur near the same time-steps as the uncertainty bound spikes from Figure 7b and Figure 8b, meaning that at these time-steps some of the Monte Carlo runs had disproportionately

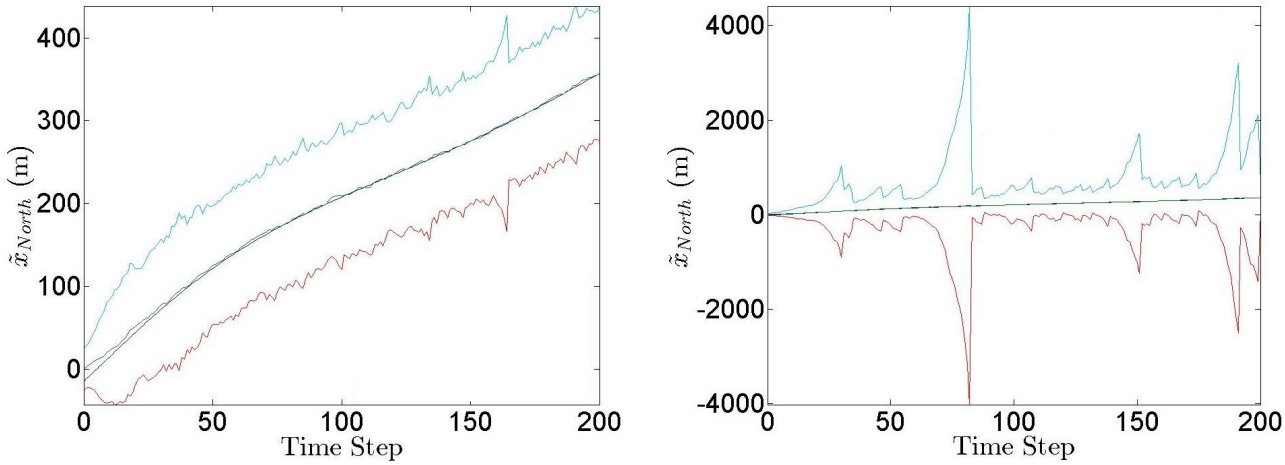

a) 5Hz **b) 2.5Hz**

Figure 7. OTDOA 1 $\tilde{x}_N$ Estimate

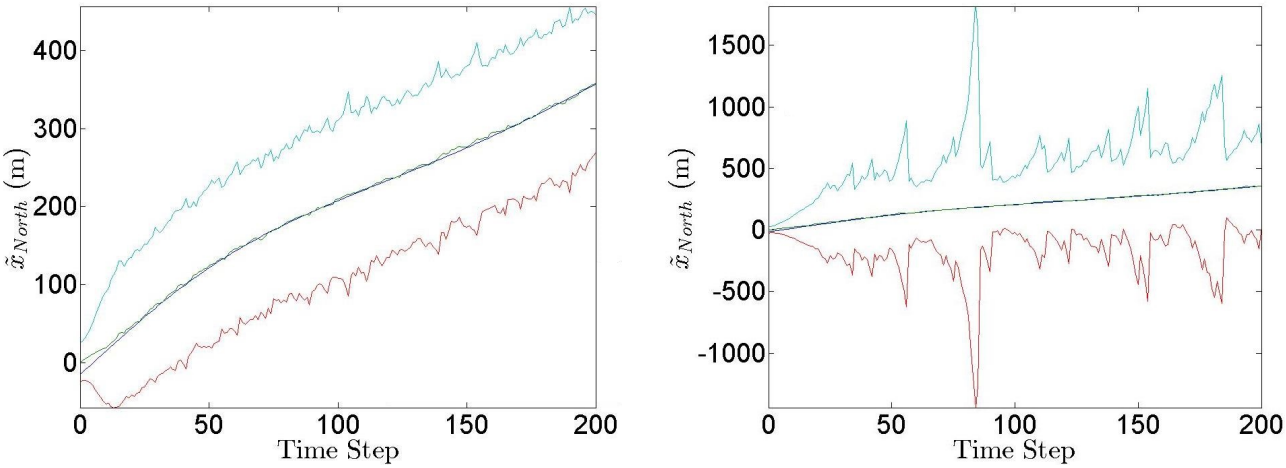

a) 5Hz **b) 2.5Hz**

Figure 8. OTDOA 2 $\tilde{x}_N$ Estimate

large errors, with wide particle distributions. This behavior is expected when measurement noise has a large covariance that can push the particle distribution to many different estimates of the state over 100 runs.

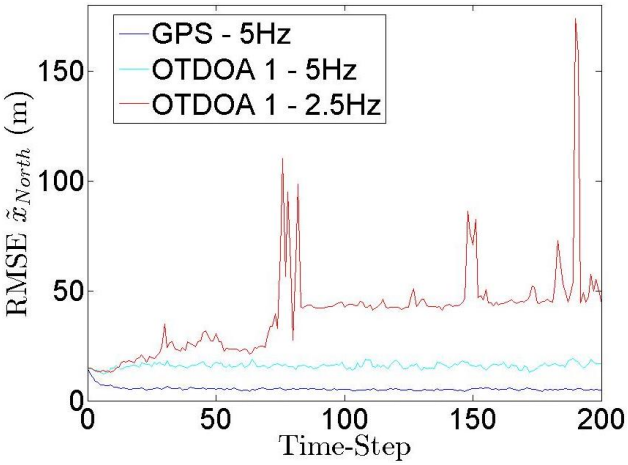

Figure 9. OTDOA 1/GPS $\tilde{x}_N$ RMS Error

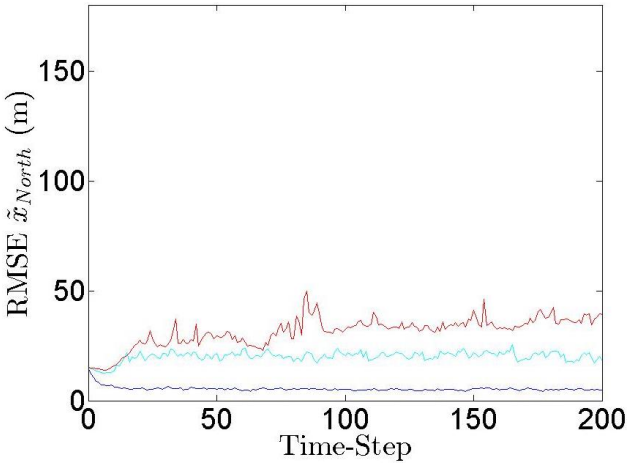

Figure 10. OTDOA 2/GPS $\tilde{x}_N$ RMS Error

B. Sensor Fusion - GPS and OTDOA

Figures 11shows the $\tilde{x}_N$ state estimate using GPS at 5Hz with OTDOA 1 at 5 Hz (Figure 11a), 2.5Hz (Figure 11b), and 1Hz (Figure 11c). Figure 12 shows the same estimates using OTDOA 2 at 5 Hz (Figure 12a), 2.5Hz (Figure 12b), and 1Hz (Figure 12c). In all cases, the state estimate mean value stays very close to the true value. The number of spikes in the uncertainty bounds increases as the OTDOA sampling rate decreases, but there are less spikes in general than in the single sensor cases. For GPS-OTDOA 1, there is one spike in the 5Hz case, two spikes in the 2.5 Hz case, and three spikes in the 1 Hz case. For GPS-OTDOA 2, there are no spikes in the 5 Hz case, two small spikes in the 2.5 Hz case, and two large spikes in the 1 Hz case. This trend in the spikes indicates that the filter is more likely to have periods of lower estimate confidence as the second sensor reports measurements with decreasing frequency. Similar to the single sensor cases, the uncertainty bounds achieve steady-state values from which the spikes deviate, and do not converge towards the state estimate, indicating that the particle distribution does not tighten as time increases.

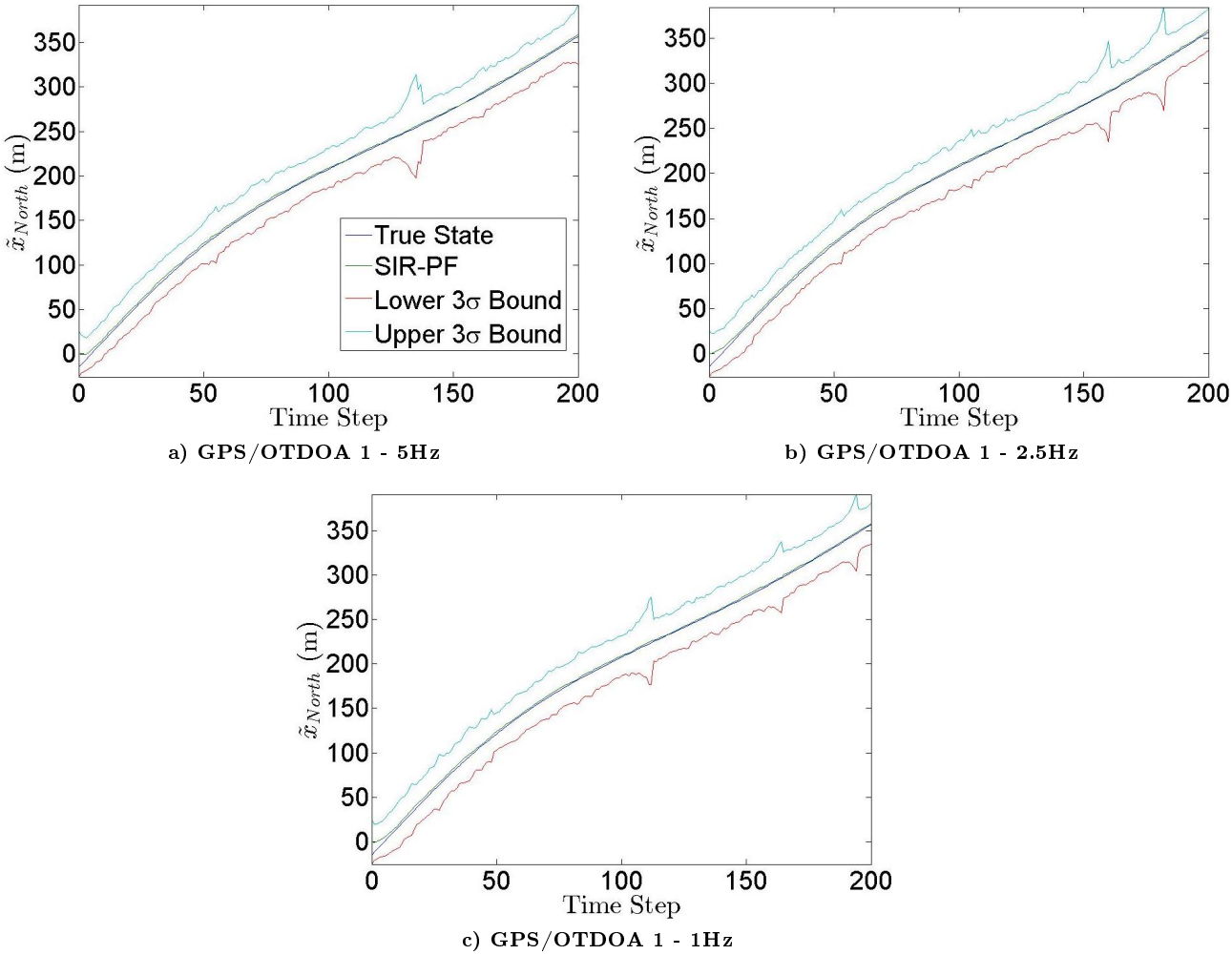

a) GPS/OTDOA 1 - 5Hz

b) GPS/OTDOA 1 - 2.5Hz

c) GPS/OTDOA 1 - 1Hz

Figure 11. GPS-OTDOA 1 $\tilde{x}_N$ Estimate

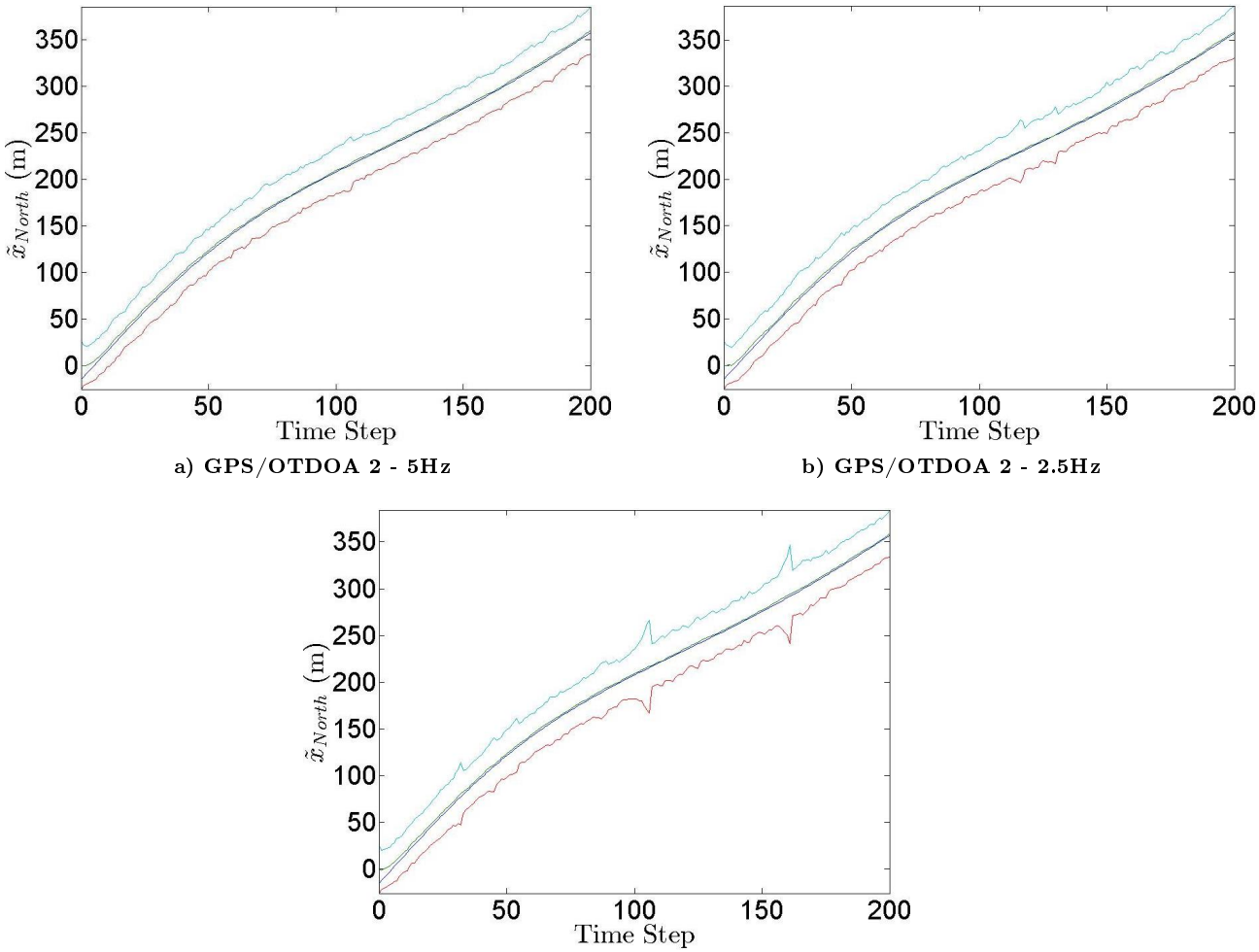

a) GPS/OTDOA 2 - 5Hz

b) GPS/OTDOA 2 - 2.5Hz

c) GPS/OTDOA 2 - 1Hz

Figure 12. OTDOA 2 $\tilde{x}_N$ Estimate

The sensor-fusion RMS error means are summarized in Table 6 with the percent change from the GPS-5Hz shown to the right of the value (black values indicate a decrease in RMS error and red values indicate an increase in RMS error). It shows slightly better RMS errors for sensor fusion combinations than the GPS single sensor in all but one case, with the improvement being larger for higher OTDOA sampling rates.

Also, for both sensor combinations at 5Hz, $\tilde{x}_E$ shows a larger improvement than $\tilde{x}_N$, while the opposite state shows larger improvement at 2.5Hz. At 1Hz, GPS/OTDOA 1 shows larger improvement for $\tilde{x}_N$ while GPS/OTDOA 2 shows larger improvement for $\tilde{x}_E$. These results further show the importance of a higher sampling rate for the second sensor in order to maintain consistency in state estimation.

Table 6. RMS Error Mean for GPS/OTDOA Fusion

	GPS/OTDOA 1		GPS/OTDOA 2	
	$\tilde{x}_N$	$\tilde{x}_E$	$\tilde{x}_N$	$\tilde{x}_E$
5Hz	5.1550 m (3.6%)	4.6833 m (7.3%)	5.1961 m (3.51%)	4.6958 m (7.07%)
2.5Hz	5.2513 m (2.48%)	5.0004 m (1.04%)	5.3042 m (1.5%)	5.0292 m (0.47%)
1Hz	5.3214 m (1.18%)	5.0664 m (-0.26%)	5.3729 m (0.23%)	4.9549 m (1.94%)

V. Conclusion and Future Work

The goal of this paper was to develop a small UAS navigation scheme able to estimate its 2-D lateral position in an urban canyon using a particle filtering method with measurements from multiple receivers.. This was accomplished by using small-UAS dynamics, sensor mean error and standard deviation characterizations for both GPS and OTDOA as well as a sampling importance resampling particle filter with particle roughening. The strongest conclusion derived from this research is that position estimates from a GPS receiver and a cellular network-enabled mobile device can be used together to provide improved navigation capabilities for a UAS in an urban canyon where GPS coverage is normally sporadic at best. Since modern mobile devices already include both technologies, there are millions of Americans carrying potential aircraft autopilots in their pockets everyday, unaware of this possibility.

Using a sampling importance resampling particle filter, this research showed that a one sensor solution will be accurate but imprecise, with the imprecision growing as a function of decreasing measurement sampling rates. The RMS error at 5Hz varies from 5.38m to 20.1m in the $\tilde{x}_N$ direction and 5.05m to 19.81m in the $\tilde{x}_E$ direction. When the GPS/OTDOA sensor combination is used at 5Hz, the RMS error, as compared to just GPS, is decreased by 3.5%-3.6% in the $\tilde{x}_N$ direction and 7.07%-7.3% in the $\tilde{x}_E$ direction. While the increase in accuracy when using OTDOA may seem trivial, this additional measurement adds robustness as cellular signals can reach deep into urban canyons that block GPS signals. The key to exploiting this data source is finding a consistent model for the OTDOA technique and more published accuracy data at varying sampling rates. Finding or collecting this experimental OTDOA data may pose a challenge since it relies on cooperation with cellular carriers and their contractors that develop proprietary TDOA geolocation solutions.

In future work, UAS flight will be simulated in a high rise urban core requiring a third sensor to provide measurements when buildings prevent GPS signal reception, since standalone OTDOA does not provide the needed accuracy and precision needed in this environment. In addition to this third sensor, process noise will be injected into the dynamics of the UAS and tuned, providing a more realistic propagation of the states.

References

[1]van Blyenburgh, P., "Unmanned Aircraft Systems: The Current Situation," *UAS ATM Integration Workshop*, UVS International, EUROCONTROL, Brussels, Belgium, May 2008.

[2]Franchi, P. L., "Law enforcement UAV requirements under study by Thales UK," *Flight International*, July 2007.

[3]Dixon, P., "Sharing the Skies," *Helicopters Magazine*, October-November-December 2011.

[4]Clarridge, C., "Seattle grounds police drone program," *The Seattle Times*, February 2013.

[5]Ma, C., Jee, G.-I., MacGougan, G., Lachapelle, G., Bloebaum, S., Cox, G., Garin, L., and Shewfelt, J., "GPS Signal Degradation Modeling," *Proceedings of the 14th International Technical Meeting of the Satellite Division of The Institute of Navigation (ION GPS 2001)*, The Institute of Navigation, Salt Lake City, UT, September 2001, pp. 882–893.

[6]Prost, J.-B., Godefroy, B., and Terrenoir, S., "Improving GPS Accuracy for Urban Pedestrians," *GPS World*, August 2008.

[7]Lu, M., Chen, W., and Chan, W. H., "Discussion of "Building project model support for automated labor monitoring" by R. Sacks, R. Navon, and E.Goldschmidt," *Journal of Computing in Civil Engineering*, Vol. 18, No. 4, 2004, pp. 381–383.

[8]Hanlon, M., "DARPA's Surface Navigation Concept - without GPS," *Gizmag*, April 2007.

[9]Schnaufer, B., "Multi-Sensor GPS Denied Navigation System and Performance for Military Operations in Urban Environments," June 2010, B.A. Schnaufer, Rockwell Collins.

[10]Haigh, N., "BAE Systems Locates Opportunity to Replace GPS," June 2012.

[11]Spirent, "An Overview of LTE Positioning," 2012, Rev. A 02/12.

[12]Ericsson, "Positioning with LTE," September 2011, 284 23-3155 Uen.

[13]Bull, J. F., "Wireless geolocation," Vol. 4, No. 4, 2009, pp. 45–53.

[14]3GPP, "3GPP TS 36.305 Technical Specification Group Radio Access Network; Evolved Universal Terrestrial Radio Access Network (E-UTRAN); Stage 2 functional specification of User Equipment (UE) positioning in E-UTRAN (Release 10)," September 2011.

[15]3GPP, "3GPP TS 36.xxx Technical Specification Group Radio Access Network; Evolved Universal Terrestrial Radio Access (E-UTRA); LTE Positioning Protocol (LPP) (Release 9)," September 2010.

[16]Tam, S., Lee, H., Khasnabish, B., and Suraci, F., "MSF Whitepaper on Location Services in LTE Networks," April 2010, White Paper.

[17]Costabile, J., "Wireless Position Location," June 2010, Slides.

[18]Mensing, C. and Plass, S., "Positioning Algorithms for Cellular Networks Using TDOA," *Acoustics, Speech and Signal Processing, 2006. ICASSP 2006 Proceedings. 2006 IEEE International Conference on*, Vol. 4, may 2006, p. IV.

[19]Yu, H., Huang, G., Gao, J., and Liu, B., "An Efficient Constrained Weighted Least Squares Algorithm for Moving Source Location Using TDOA and FDOA Measurements," Vol. 11, No. 1, 2012, pp. 44–47.

[20]Bucher, R. and Misra, D., "A Synthesizable VHDL Model of the Exact Solution for Three-dimensional Hyperbolic Positioning System," *Vlsi Design*, Vol. 15, No. 2, 2002, pp. 507–520.

[21]Ranta-aho, K., "Performance of 3GPP Rel-9 LTE positioning methods," June 2010, Slides.

[22]Möckli, M. R., ., *Guidance and Control for Aerobatic Maneuvers of an Unmanned Airplane*, Ph.D. thesis, Swiss Federal Institute of Technology Zurich, 2006.

[23]Gordon, N., Salmond, D., and Smith, A., "Novel approach to nonlinear/non-Gaussian Bayesian state estimation," *IEEE Proceedings F, Radar and Signal Processing*, Vol. 140, No. 2, 1993, pp. 107–113.

[24]Thrun, S., Burgard, W., and Fox, D., *Probabilistic Robotics (Intelligent Robotics and Autonomous Agents)*, The MIT Press, 2005.

[25]Arulampalam, M., Maskell, S., Gordon, N., and Clapp, T., "A tutorial on particle filters for online nonlinear/non-Gaussian Bayesian tracking," *Signal Processing, IEEE Transactions on*, Vol. 50, No. 2, feb 2002, pp. 174 –188.

[26]Doucet, A., Godsill, S., and Andrieu, C., "On sequential Monte Carlo sampling methods for Bayesian filtering," *Statistics and computing*, Vol. 10, No. 3, 2000, pp. 197–208.

[27]Ristic, B., Arulampalm, S., and Gordon, N., *Beyond the Kalman filter: Particle filters for tracking applications*, Artech House Publishers, 2004.

[28]Carpenter, J., Clifford, P., and Fearnhead, P., "Improved particle filter for nonlinear problems," *IEE Proceedings-Radar, Sonar and Navigation*, Vol. 146, No. 1, 1999, pp. 2–7.

[29]Khan, T., Ramuhalli, P., and Dass, S., "Particle-Filter-Based Multisensor Fusion for Solving Low-Frequency Electromagnetic NDE Inverse Problems," *Instrumentation and Measurement, IEEE Transactions on*, Vol. 60, No. 6, june 2011, pp. 2142 –2153.

[30]Soysal, G. and Efe, M., "Data fusion in a multistatic radar network using covariance intersection and particle filtering," *Information Fusion (FUSION), 2011 Proceedings of the 14th International Conference on*, IEEE, 2011, pp. 1–7.

[31]Electronics, S., "66 Channel LS20031 GPS 5Hz Receiver," .

[32]Wireless, P., "Wireless Location Technology Overview," White Paper, January 2012.

[33]MacGougan, G., Lachapelle, G., Klukas, R., Siu, K., et al., "Degraded GPS Signal Measurements With A Stand-Alone High Sensitivity Receiver," *Presented at ION National Technical Meeting*, Vol. 28, 2002, p. 30.

[34]Ahonen, S., Lähteenmäki, J., Laitinen, H., and Horsmanheimo, S., "Usage of mobile location techniques for UMTS network planning in urban environment," 2002.

[35]Neuland, M., Kurner, T., and Amirijoo, M., "Influence of Positioning Error on X-Map Estimation in LTE," *Vehicular Technology Conference (VTC Spring), 2011 IEEE 73rd*, may 2011, pp. 1 –5.

[36]Tao, S., "Mobile Phone-based Vehicle Positioning and Tracking and Its Application in Urban Traffic State Estimation," 2012, QC 20111206.

[37]Matthews, J. H., "Module for Runge Kutta Method for O.D.E.'s," 2003.